Reac Kinet Mech Cat (2016) 117:503–520
DOI 10.1007/s11144-015-0947-8

Kinetic and activity study of CO oxidation over CuO–MnO_x–CeO_2 catalysts

Ai-Ping Jia[1] · Yun Deng[1] · Geng-Shen Hu[1] · Meng-Fei Luo[1] · Ji-Qing Lu[1]

Received: 27 July 2015 / Accepted: 1 November 2015 / Published online: 13 November 2015

Abstract Three CuO–MnO_x–CeO_2 catalysts with different impregnation sequences (i.e. MnO_x/CuO/CeO_2, CuO/MnO_x/CeO_2 and CuO–MnO_x/CeO_2) were prepared and the effects of impregnation sequences on the structures and catalytic behaviors of these catalysts were investigated. It was found that the MnO_x/CuO/CeO_2 possessed the largest amount of oxygen vacancies but the lowest reducibility; the CuO/MnO_x/CeO_2 had the largest Cu^+ contents but the lowest amount of oxygen vacancies; the CuO–MnO_x/CeO_2 catalyst had the highest CuO dispersion and the best reducibility, along with moderate amount of oxygen vacancies and Cu^+ contents on the surface. The kinetic studies revealed that the apparent activation energies of CO oxidation over the CuO–MnO_x/CeO_2, MnO_x/CuO/CeO_2 and CuO/MnO_x/CeO_2 were 49.5, 51.8 and 73.8 kJ mol^{-1}, in order, and the activities followed an order of CuO–MnO_x/CeO_2 > MnO_x/CuO/CeO_2 > CuO/MnO_x/CeO_2. The highest performance of the CuO–MnO_x/CeO_2 was ascribed to the highly dispersed CuO species and the mobility of lattice oxygen.

Keywords CO oxidation · CuO–MnO_x–CeO_2 catalysts · CuO dispersion · Oxygen vacancy · Kinetics

Electronic supplementary material The online version of this article (doi:10.1007/s11144-015-0947-8) contains supplementary material, which is available to authorized users.

✉ Ji-Qing Lu
jiqinglu@zjnu.cn

[1] Key Laboratory of the Ministry of Education for Advanced Catalysis Materials, Institute of Physical Chemistry, Zhejiang Normal University, Jinhua 321004, China

Introduction

Carbon monoxide (CO) is generally produced and released from fossil fuel combustion, and its removal is highly necessary in industrial applications. Recently, preferential CO oxidation (PROX) [1–3] has triggered a lot of interests in the application of PEMFC. In the past decades, both noble metals and transition metal oxides have been widely studied for CO oxidation. Although it is generally recognized that noble metals (i.e. Au, Pt, Pd and Rh) [4–7] are the most effective catalysts for CO oxidation, their applications might be limited by the high costs and easy deactivation. Alternatively, CuO/CeO_2 catalysts were found to be excellent candidates due to their low costs and high activities [8], and, therefore, they have been widely applied in CO oxidation or CO-PROX [1, 9–12]. The catalytic performances of the $CuO–CeO_2$ catalysts are mainly attributed to the high oxygen storage/release capability of CeO_2 via the redox couple of Ce^{4+}/Ce^{3+} and the strong interaction between copper oxides and ceria.

Continuous efforts have been made to improve the efficiencies of the CuO/CeO_2 catalysts. A general approach is the addition of other active components to the catalyst. For example, the addition of Zr^{4+} [13, 14] and Sn^{4+} [15] in the lattice of CeO_2 could increase the mobility of lattice oxygen and enhance the CO selective oxidation activity. Besides, the addition of α-Fe_2O_3 could also promote the reactivity of Cu–Ce–Fe–O catalysts [16]. Recently, CuO/CeO_2 catalysts modified with manganese have been reported for CO-PROX [17–21]. Li et al. [17, 18] reported that doping proper amount of Mn into $CuO–CeO_2$ catalysts would improve the catalytic performance for CO-PROX reaction, owing to the formation of a more stable Cu–Mn–Ce–O solid solution and the enhancement of the redox properties of catalysts. Tang et al. [22] showed that the addition of copper significantly improved the catalytic activity of $MnO_x–CeO_2$ mixed oxide in the complete oxidation of benzene. Recently, Gong et al. [21] reported a series of $CuO/CeO_2–MnO_x$ with different atomic Mn/(Ce + Mn) ratios, among which the catalyst with a Mn/Ce + Mn atomic ratio of 0.4 was the most active due to a larger BET surface area and more highly dispersed copper oxides on the surface. However, detailed kinetic studies on these catalysts were absent, and thus some essential information on the intrinsic properties of these catalysts could not be provided.

In addition, the activity of the catalyst strongly depends on not only chemical composition of catalysts, but also preparation methods. Even changing the impregnation sequence of components can make an effect on the catalytic performance. For example, Zhang et al. [23] reported that the impregnation sequence of Ir and Fe species on the Al_2O_3 support had a remarkable effect on the catalytic performance for CO oxidation. In the current work, three types of $CuO–MnO_x–CeO_2$ catalysts with different impregnation sequences of CuO and MnO_x were prepared. It was found that the impregnation sequence of CuO and MnO_x obviously affected the overall CO oxidation activities of the $CuO–MnO_x–CeO_2$ catalysts. Detailed kinetic studies were performed on these catalysts to investigate their intrinsic behavior. Based on these results, a correlation between the properties

of the catalysts (such as CuO dispersion, the amount of oxygen vacancy, reducibility and the Cu^+ content) and the catalytic performance was established.

Experimental

Catalyst preparation

The CeO_2 support was prepared using a precipitation method. In a typical synthesis, 25.23 g of $Ce(NO_3)_3{\cdot}6H_2O$ (58.1 mmol) was completely dissolved in deionized water (500 ml), and then a certain quantity of $NH_3{\cdot}H_2O$ solution was gradually added to the solution until the pH of solution was adjusted to about 11.0 to form a precipitate. The precipitate was stirred at 40 °C for 8 h and then aged at 100 °C overnight. Then it was filtered, repeatedly washed with deionized water and dried at 100 °C overnight, followed by calcination at 400 °C for 4 h. The resulting CeO_2 powder had a surface area of 58 $m^2\ g^{-1}$, as determined by N_2 sorption at 77 K.

The supported CuO–MnO_x–CeO_2 catalysts were prepared by impregnating aqueous solutions of $Cu(NO_3)_2$ and $Mn(NO_3)_2$ with the CeO_2 support. In the preparation procedure of the $MnO_x(5)/CuO(5)/CeO_2$ catalyst, an aqueous solution of $Cu(NO_3)_2$ was impregnated onto the CeO_2 support. The slurry was heated at 90 °C under stirring for 15 min to remove the water, followed by calcination at 400 °C for 4 h in air. Then the obtained CuO/CeO_2 powder was immersed in a certain quantity of $Mn(NO_3)_2$ solution, and followed the same procedure as described. The obtained catalyst was designated as $MnO_x(5)/CuO(5)/CeO_2$ with the number referring to the weight percentage of MnO_x (nominally MnO_2) or CuO in the catalyst. For the $CuO(5)/MnO_x(5)/CeO_2$ catalyst, the preparation process is similar to that of the $MnO_x(5)/CuO(5)/CeO_2$, but with the impregnation of $Mn(NO_3)_2$ first and then the Cu $(NO_3)_2$. For the CuO(5)–$MnO_x(5)/CeO_2$ catalyst, a mixed aqueous solution of $Cu(NO_3)_2$ and $Mn(NO_3)_2$ was impregnated onto the CeO_2 support, which was heated at 90 °C under stirring for 15 min to remove the water, followed by calcination at 400 °C for 4 h in air. In addition, two monometallic catalysts $CuO(10)/CeO_2$ and $MnO_x(10)/CeO_2$ were also prepared with a similar manner.

Characterization

X-ray diffraction (XRD) patterns were collected on a PANalytic X'Pert PRO MPD powder diffractometer using Cu K_α radiation ($\lambda = 0.1542$ nm). The working voltage was 40 kV and the working current was 40 mA. The patterns were collected in a 2θ range from 10° to 110° with a scan rate of 0.15° s^{-1}. The lattice parameter was determined by the Rietveld method using JADE 6.5 software.

Raman measurements were performed on a Renishaw RM1000 with a confocal microprobe, using excitation laser line of 514 nm. Data acquisition was carried out at 25 °C with the scanning range from 200 to 2000 cm^{-1}.

The reducibility of the catalyst was measured by H_2 temperature-programmed reduction (H_2-TPR) technique. 50 mg of the catalyst was placed in a quartz reactor

and heated from 50 to 450 °C with a heating rate of 10 °C min^{-1} in a gas mixture (5 % H_2 in N_2, 30 ml min^{-1}). In order to remove adsorbed oxygen and water in the catalyst, the catalyst was subjected to a flow of He (30 ml min^{-1}) at 300 °C for 0.5 h before the experiment. The amount of H_2 consumption was determined by a gas chromatograph with a TCD detector, calibrated by the reduction of a known amount of CuO powder.

The X-ray photoelectron spectroscopy (XPS) measurements were performed on an ESCALAB 250Xi high performance electron spectrometer using Mg K_α excitation source ($h\nu = 1253.6$ eV) of the twin anode in this work. The pass energies of 150.0 and 10.0 eV were used for recording survey and high-resolution spectra, respectively. Binding energies were calibrated by using the contaminant carbon (C1s = 284.8 eV). The XPS analysis was done at room temperature and pressures on the order of 10^{-9} mbar. The spectra were deconvoluted using the Avantage software 5.926.

In situ Fourier transform infrared (FTIR) spectra of CO chemisorption over the catalysts were recorded on a NEXUS670 spectrometer equipped with a MCT detector. Self-supported sample wafers (diameter = 1 cm) were prepared from 30 mg of catalyst by pressing at about 3 MPa. The sample was transferred to a quartz IR cell connected to the closed circulation systems and then pretreated under a He flow (30 ml min^{-1}) at 300 °C for 1 h in order to remove water and carbonate in the catalyst. After the pretreatment, the sample was cooled down to 30 °C and the gas mixture (1 % CO in N_2, 10 ml min^{-1}) was introduced to the IR cell and the sample was heated from 30 to 300 °C at a ramp of 10 °C min^{-1}. The catalyst was purged with pure He for 30 min to remove the gaseous and physisorbed CO and then a spectrum was collected.

Catalytic testing

The reaction was carried out in a quartz tubular (6 mm i.d.) fixed-bed reactor under atmospheric pressure. 100 mg of catalyst (100–120 mesh) was loaded in the reactor and the reaction temperature was monitored by a thermocouple placed in the middle of the catalyst bed. A feed gas consisting of 1 % CO and 1 % O_2 in N_2 with a total flow rate of 80 ml min^{-1}, corresponding to a space velocity of 48,000 ml g_{cat}^{-1} h^{-1}, was introduced as the reactants. The catalyst was directly exposed to reaction gas without any pretreatment. The CO concentration of the reactor effluent was analyzed using an Agilent 6850 gas chromatograph equipped with a TCD detector attached to an HP PLOT (30 m × 0.32 mm × 12 μm) column.

Reaction kinetics

The kinetic study was performed on the same fixed bed reactor as mentioned in the catalytic testing. The reaction conversion was controlled by reaction temperature since the loading of the catalyst in each experiment was kept at 50 mg, diluted with same weight of quartz sand. The diluted catalyst was embedded with glass wool on both sides. A thermocouple was inserted into the middle of the catalyst bed to monitor the reaction temperature. In this kinetic experiment, the concentration of

CO or O_2 in the feed was varied between 0.3 and 3 %. Each measurement was taken after stable rate was achieved, which took about 1 h. Separate experimental tests showed that both external and internal mass transfer could be eliminated using a gas flow rate of 120 ml min^{-1} and catalyst particles smaller than 100–120 mesh, which therefore were employed for the kinetic study. The absence of mass and heat transfer limitation was verified by checking the Weisz–Prater criterion and Mears' criterion [24] as applied in our previous work [9]. The kinetic study was conducted at 80 °C for all these catalysts based on that their CO conversion was not exceeding 10 % under these temperatures. CO_2 concentration in the outlet gas stream was also analyzed by the same Agilent 6850 gas chromatograph mentioned above. The calculation of CO conversion and the power-rate law expressions were described elsewhere [9].

Results and discussion

Catalyst characterizations

X-ray diffraction (XRD)

The XRD patterns of the CuO–MnO_x–CeO_2 catalysts are shown in Fig. S1 (see Fig. S1 in Supplementary Information) and their lattice parameters extracted from the patterns are listed in Table 1. All these catalysts have characteristic peaks of fluorite-type oxide structure of CeO_2. In addition, two peaks characteristic of CuO phase at 35.5° and 38.8° are detected in the CuO-containing catalysts (except for the CuO(5)–MnO_x(5)/CeO_2), arising from the aggregation of copper species on the surface of ceria. For the CuO(5)–MnO_x(5)/CeO_2 catalyst, no crystalline peaks of copper species are observed, which suggests that copper species are highly dispersed on the ceria surface in an amorphous phase and/or incorporated into ceria lattice to form ceria-based solid solution. In other words, the co-impregnation of MnO_x with CuO leads to an increase of the CuO dispersion on the surface of supports as confirmed by the patterns. On the other hand, no diffraction peaks corresponding to manganese oxides are found, suggesting that the manganese oxides are highly dispersed or poorly crystallized [25] or combined with the finely dispersed copper oxide and ceria to form solid solution [26]. It can be seen in Table 1 that the lattice parameters of CuO–MnO_x–CeO_2 catalyst decrease slightly compared to that of pure CeO_2. This finding suggests that a small amount of Cu–Mn–Ce–O solid solution [27, 28] could be formed in these catalysts due to the partial substitution of Ce^{4+} by Cu^{2+} and/or Mn^{x+} ions since smaller ionic radii (the radii of Cu^{2+}, Mn^{4+}, Mn^{3+} and Mn^{2+} are 0.073, 0.056, 0.062 and 0.067 nm) than that of Ce^{4+} (0.097 nm). Such a contraction of the lattice leads to a bigger strain, which enhances the generation of oxygen vacancies in the samples and thus improves the redox properties of CeO_2 [29].

Table 1 Lattice parameters, H_2 consumption, molar contents of O, Mn and Cu species and surface compositions in various catalysts

Catalysts (%)	Lattice parameters (nm)	H_2 consumption (μmol g^{-1})		O1s molar content (%)		$Mn2p_{3/2}$ molar content (%)		$Cu2p_{3/2}$ molar content		Surface composition	
		Actual	Nominal[a]	O_{latt}	O_{ads}	Mn^{3+}	Mn^{4+}	Cu^{+}	Cu^{2+}	Cu/(Cu + Mn + Ce)	Mn/(Cu + Mn + Ce)
$MnO_x(5)/CuO(5)/CeO_2$	0.5411 (8)	1300	1201	53.6	46.4	47.1	52.9	58.1	41.9	0.31	0.15
$CuO(5)/MnO_x(5)/CeO_2$	0.5410 (8)	1370	1201	61.6	38.4	56.5	43.5	76.0	24.0	0.44	0.05
$CuO(5)–MnO_x(5)/CeO_2$	0.5411 (4)	1530	1201	59.9	40.1	55.3	44.7	60.2	39.8	0.45	0.06
$CuO(10)/CeO_2$	0.5411 (6)	1640	1250	65.2	34.8	–	–	63.9	36.1	–	–
$MnO_x(10)/CeO_2$	0.5411 (4)	1280	1151	64.2	35.8	56.7	43.3	–	–	–	–
CeO_2	0.5412 (3)	20	–	67.0	33.0	–	–	–	–	–	–

[a] The x in MnO_x was estimated to be 2

Raman spectroscopy

To obtain further information on the structural features, the catalysts were examined by Raman spectroscopy, as shown in Fig. 1. All the catalysts have two distinct bands at 463 and 612 cm^{-1}. The band at 463 cm^{-1} is ascribed to the F_{2g} vibration mode of fluorite structure of CeO_2 [30]. A slight red shift is also observed in the fluorite F_{2g} band for the CuO–MnO_x–CeO_2 catalysts, which is related to the incorporation of a small amount of Cu^{2+} and/or Mn^{x+} ions to the fluorite lattice [31]. The bands at 612 cm^{-1} are related to oxygen vacancies in the fluorite ceria lattice [32], which is generated from the formation of the Cu–Mn–Ce–O solution and charge compensation for the partial replacement of Ce^{4+} ions by the Cu^{2+} [33] and/or Mn^{x+}. However, it should be noted that the feature band of MnO_2 is located at 588 cm^{-1} [34], the observed peak at 612 cm^{-1} may contain some contribution from the MnO_2. In order to compare the relative amount of oxygen vacancies present in the catalysts, the peak areas of the bands at 463 and 612 cm^{-1} are calculated based on the results shown in Fig. 1, which are denoted as A_{463} and A_{612}, respectively. The ratios of A_{612}/A_{463}, which reflect the relative concentrations of oxygen vacancies in the catalysts [29], are also shown in Fig. 1. It can be seen that

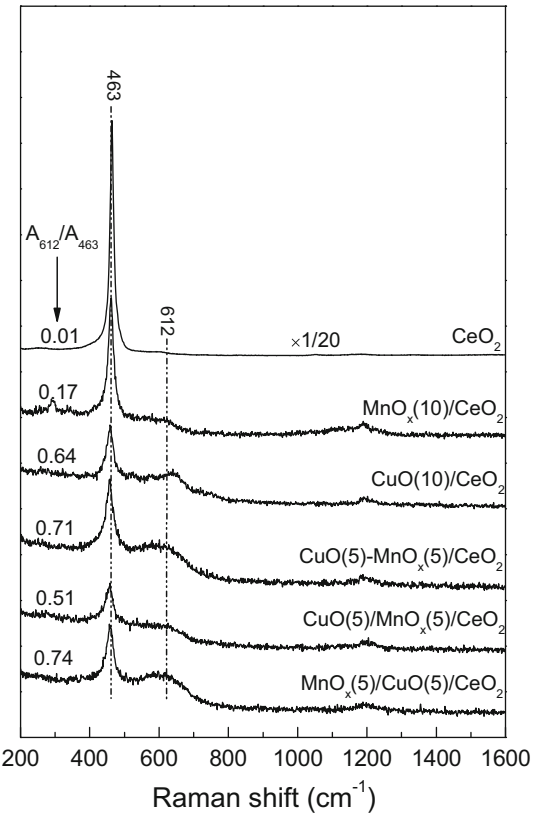

Fig. 1 Raman spectra of various catalysts

the pure CeO_2 has a value of 0.01, while the supported catalysts have higher ratios. The higher A_{612}/A_{463} ratios on the supported catalysts strongly suggest that Cu^{2+} and/or Mn^{n+} ions penetrate into the CeO_2 matrix, leading to the formation of extra oxygen vacancies in these catalysts. In addition, note that the $MnO_x(5)/CuO(5)/CeO_2(0.74)$ catalyst has the largest ratio compared to the $CuO/MnO_x(5)/CeO_2$ (0.51) and the $CuO(5)–MnO_x(5)/CeO_2$ (0.71) catalysts, implying that the $MnO_x(5)/CuO(5)/CeO_2$ catalyst has the largest amount of oxygen vacancies.

Reducibility

Fig. S2 in the Supplementary Information presents the H_2-TPR profiles of various catalysts and their H_2 consumptions (calibrated by known amount of pure CuO powder) are listed in Table 1. The pure CeO_2 is barely reduced below 450 °C (with a H_2 consumption of 20 μmol g^{-1}), which is assigned to the reduction of surface CeO_2. The H_2-TPR profile of the $MnO_x(10)/CeO_2$ exhibits two overlapping reduction peaks at 275 and 344 °C, which is similar to that of pure MnO_x [20]. This reduction is assigned to the two-step reduction of MnO_x (MnO_2/Mn_2O_3) to Mn_3O_4, and Mn_3O_4 to MnO. However, the reduction temperatures of the MnO_x/CeO_2 are much lower than those of pure MnO_x, which indicates synergistic promotion between MnO_x and CeO_2 in the reduction of the catalysts. As for the $CuO–MnO_x–CeO_2$ catalysts, two reduction peaks shift to lower temperature at 190 and 210 °C due to the spillover process promoted by $CuO–CeO_2$ interfacial sites, which are attributed to the overlapped reduction of CuO and MnO_x together with Cu^{2+} and/or Mn^{x+} ions in the CeO_2 lattice [9]. However, these reduction temperatures are slightly higher than those of the $CuO(10)/CeO_2$, which shows three overlapping reduction peaks at 169, 189 and 222 °C. The reduction peak at 169 °C is associated to copper oxide in strict contact with ceria, i.e. to Cu–O–Ce sites [35]. The other two peaks are due to reduction of bulk CuO with different sizes [9]. The H_2 consumption of each catalyst is given in Table 1. For all the catalysts, the total hydrogen consumption for $CuO–MnO_x–CeO_2$ reduction exceeds the theoretical values, which imply a simultaneous reduction of metal oxide species and support by means of hydrogen spillover and that incorporating Cu and Mn into the CeO_2 lattice to form a solid solution facilitated the release of the lattice oxygen. According to the results in Table 1, $CuO(5)–MnO_x(5)/CeO_2$ has the highest amount of H_2 consumption, the $CuO(5)/MnO_x(5)/CeO_2$ has the medium while the $MnO_x(5)/CuO(5)/CeO_2$ has the lowest. These results suggest that the $CuO(5)–MnO_x(5)/CeO_2$ possesses the best reducibility or oxygen mobility, probably due to its highly dispersed surface species (CuO and MnO_x) and strong interaction between the metal oxides and and the CeO_2 support.

Oxidation state analysis

Oxidation states of the surface species are analyzed by XPS, as shown in Fig. S3 and Fig. 2. Fig. S3 in the Supplementary Information shows the XPS spectra of the Ce3d (Fig. S3a) and O1s (Fig. S3b) of the $CuO(5)–MnO_x(5)–CeO_2$ catalysts. The Ce3d XPS spectra show multiple states arising from different Ce4f level occupancies in

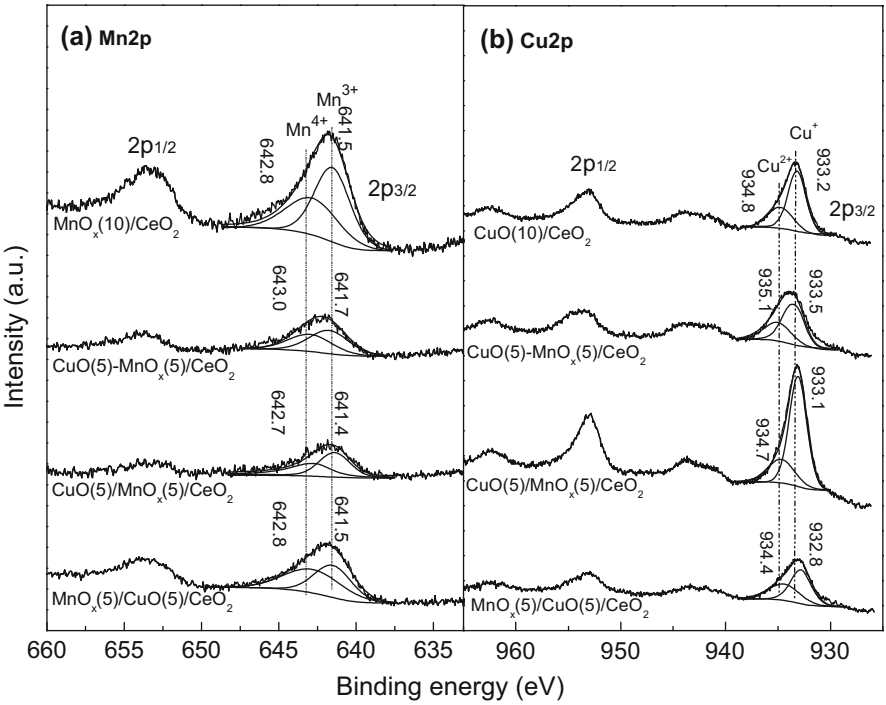

Fig. 2 **a** Mn2p and **b** Cu2p XPS spectra of various catalysts

the final state [36]. According to the literature [37], the curves of Ce 3d spectra are composed of six peaks corresponding to three pairs of spin–orbit doublets. Letters U and V refer to the $3d_{3/2}$ and $3d_{5/2}$ spin–orbit doublets, respectively. The peaks labeled as U′ (ca.900.8 eV), U″ (ca.908.0 eV) and U‴ (ca.916.4 eV) result from Ce^{4+} $3d_{3/2}$ while V′ (ca.882.4 eV), V″ (ca.888.2 eV) and V‴ (ca.898.3 eV) result from Ce^{4+} $3d_{5/2}$. Unfortunately, no peak ascribed to the Ce^{3+} ion was observed probably due to the reason that the signal of Ce^{3+} is too weak and overlapped by the peak of Ce^{4+}. In other words, the Ce species in all CeO_2 based catalysts are mostly Ce^{4+}. Fig. S3b displays the O1s XPS spectra of CuO(5)–MnO_x(5)–CeO_2 catalysts, in which two oxygen species can be distinguished. The lower binding energy at 529.0–529.4 eV was attributed to the lattice oxygen (denoted as O_{latt}), while the higher binding energy at 530.7–531.3 eV was assigned to surface adsorbed oxygen (denoted as O_{ads}) with low coordination [22]. Compared with the CuO(10)/CeO_2, MnO_x(10)/CeO_2 and CeO_2 support, the bimetallic CuO–MnO_x–CeO_2 catalysts has relatively higher concentration of O_{ads} as shown in Table 1, which are favorable for the mobility of oxygen species and transferring to lattice oxygen via oxygen vacancy [19]. Among these, the MnO_x(5)/CuO(5)/CeO_2 has the highest concentration of adsorbed surface oxygen (O_{ads}), while the CuO–MnO_x(5)/CeO_2 has the medium and CuO(5)/MnO_x(5)/CeO_2 has the lowest, following the same sequence of A_{612}/A_{463} as displayed in Fig. 1.

For the Mn 2p spectra (Fig. 2a), the main peaks of the Mn $2p_{3/2}$ could be deconvoluted into two components centered at 641.5 and 642.8 eV, which can be assigned to Mn^{3+} and Mn^{4+}, respectively. As listed in Fig. 2a, it is found that the binding energy (BE) of $Mn2p_{3/2}$ (Mn^{3+} and Mn^{4+}) in the CuO(5)–MnO_x(5)/CeO_2 is 0.3 eV higher than that of MnO_x(5)/CuO(5)/CeO_2 or the CuO(5)/MnO_x(5)/CeO_2 catalyst, which are essentially identical to that of the MnO_x(10)/CeO_2 catalyst, indicating an stronger interaction between the MnO_x and CuO or CeO_2 in the CuO(5)–MnO_x(5)/CeO_2 catalyst. Fig. 2b shows the Cu 2p XPS of the CuO–MnO_x–CeO_2 catalysts. The main peaks of Cu $2p_{3/2}$ core level could be deconvoluted into two components located at 932.2 eV attributed to Cu^+ species and 934.8 eV assigned to Cu^{2+} species, along with the shake-up peak above Cu^{2+} species at 942.1 eV [38], suggesting the presence of copper species in forms of Cu^{2+} and Cu^+. Also, the $Cu2p_{2/3}$ peak shifts to higher energy compared with that of the CuO(10)/CeO_2 catalyst, which implies a strong interaction between CuO and MnO_x or the CeO_2 support. Surface concentrations of Cu and Mn species listed in Table 1 reveal that the CuO(5)/MnO_x(5)/CeO_2 contains the highest amount of Cu^+ (76 %) and the lowest amount of Mn^{4+} (about 43.5 %), indicating that an electron transfer process may exist between Mn and Cu species. In the CuO(5)/MnO_x(5)/CeO_2 catalyst, the Cu^{2+} are probably most facile to accept electrons provided by Mn species, resulting in the formation of the highest amount Cu^+. These results indicate that the capability of the redox couple Cu^{2+}–Cu^+ in the catalyst may be strongly enhanced by a large number of Mn^{4+} ions existing on the surface of CeO_2 [39]. As reported by Liu et al. [40], there was a strong interaction between copper, manganese and the support via charge transfer.

The surface contents of Cu and Mn as well as surface composition ratios derived by XPS are also summarized in Table 1. The ratios verify that the CuO(5)/MnO_x(5)/CeO_2 catalysts possesses the highest amount of exposed surface CuO species among three CuO–MnO_x–CeO_2 catalysts, while the MnO_x(5)/CuO(5)/CeO_2 has the least. The surface Cu/(Cu + Mn + Ce) atomic ratios for the MnO_x(5)/CuO(5)/CeO_2, CuO(5)/MnO_x(5)/CeO_2 and CuO(5)–MnO_x(5)/CeO_2 catalysts are 0.31, 0.44 and 0.45, in order. This implies that the CuO(5)–MnO_x(5)/CeO_2 has the highest dispersion of Cu species, which is consistent with the XRD results.

FTIR spectra of CO chemisorption

Fig. 3 presents the FTIR spectra of CO chemisorption on the catalysts at 80 °C. It is found that the pure CeO_2 support and MnO_x(10)/CeO_2 cannot chemisorb CO. For all the CuO-containing catalysts, bands at 2110 cm^{-1} are clearly observed. This characteristic band could be assigned to linear chemisorption of CO on Cu^+ (Cu^+-carbonyl) [11]. The formation of the Cu^+ species may be caused by three facts. First, Cu^+ species naturally coexists with Cu^{2+} in the CuO–MnO_x–CeO_2 catalysts as demonstrated by our XPS results listed in Table 1. Second, Cu^+ species are formed as a result of reduction of Cu^{2+} by CO when the CuO–MnO_x–CeO_2 catalysts are subjected to a mixture of CO and O_2. Martínez-Arias et al. [41] reported that for a fully oxidized CuO–CeO_2 catalyst, around 70 % of Cu^{2+} was

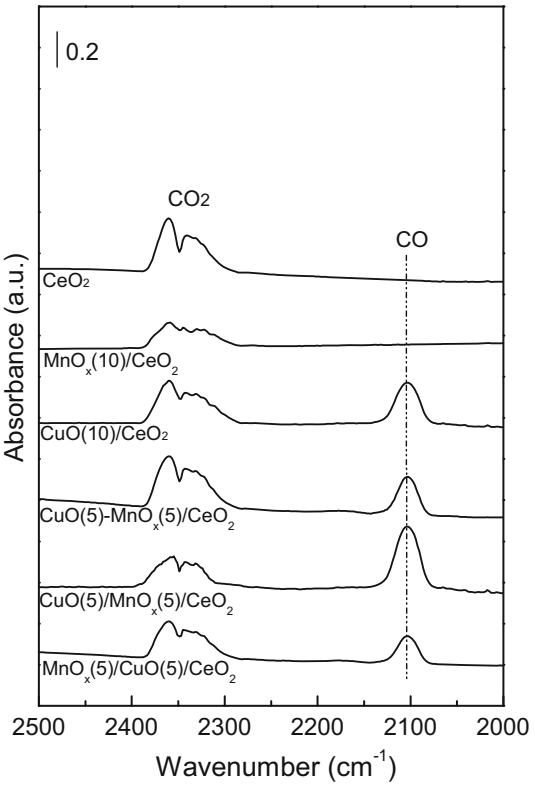

Fig. 3 FTIR spectra for CO chemisorption on various catalysts at 80 °C

reduced to Cu^+ by 1 Torr CO even at 300 K and the Cu^+ state remains unchanged under 1 Torr O_2 at 373 K, indicating a stabilized Cu^+ valance state on the catalyst. Third, the formation of another part of Cu^+ species is related to the redox process between Cu and Mn species at interfacial position of CuO–MnO_x, which could transfer electrons from Mn^{3+} to Cu^{2+} to form Cu^+, as confirmed by the XPS results (Table 1).

Kinetic study

The kinetic study of CO oxidation was performed over the three types of CuO–MnO_x–CeO_2 catalysts. By changing the partial pressures of CO and O_2, a series of CO conversions were obtained and consequently reaction rates in unit of $mol_{CO}\ g_{cat}^{-1}\ s^{-1}$ were calculated. Fig. 4 shows the variation of CO oxidation rates over the CuO–MnO_x(5)/CeO_2, MnO_x(5)/CuO(5)/CeO_2 and CuO(5)–MnO_x(5)/CeO_2 catalysts. For all the catalysts, the reaction rate increases nonlinearly with P_{CO} under constant P_{O_2} (Fig. 4a), but hardly changes with P_{O_2} (Fig. 4b) under constant P_{CO}. The results of the non-linear regression using the POLYMATH 5.1 program for the reaction rates of CO oxidation over CuO–MnO_x(5)/CeO_2, MnO_x(5)/CuO(5)/CeO_2 and CuO(5)–MnO_x(5)/CeO_2 catalysts are given in Table 2. The CO pressure

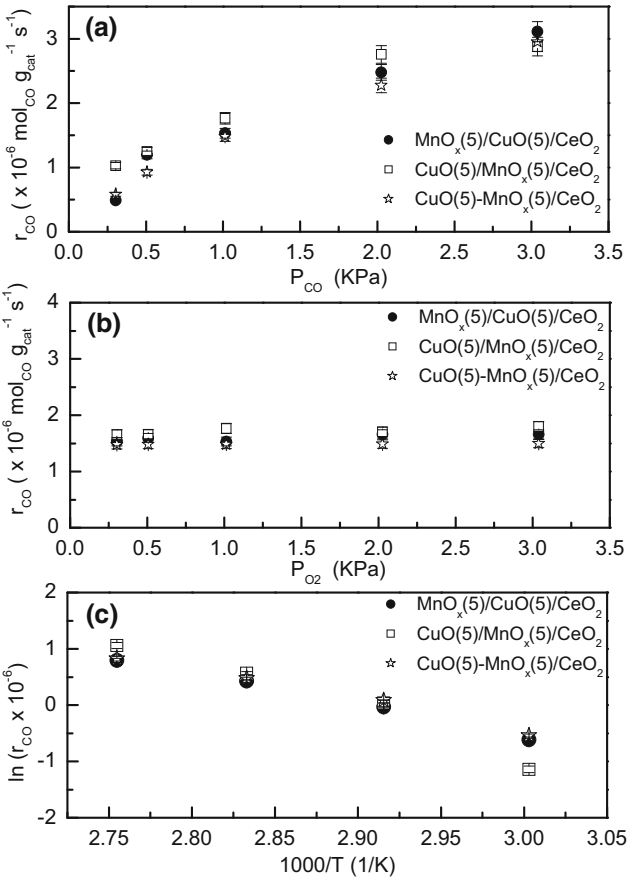

Fig. 4 Variation of CO oxidation rate and Arrhenius plots of CO reaction rates over various catalysts with partial pressures of CO under 1 % O_2 or O_2 under 1 % CO (R^2 is the correlation coefficient). Reaction condition: 50 mg catalyst diluted with the same weight of quartz sand (100–120 mesh), the concentration of CO or O_2 was varied between 0.3 and 3 %, T = 80 °C

Table 2 Summary of kinetics results for CO oxidation over various catalysts

Catalyst	Power rate expression	E_a (kJ mol^{-1})
$MnO_x(5)/CuO(5)/CeO_2$	$r = kP_{CO}^{0.72}P_{O_2}^{0.043}$	51.8
$CuO(5)/MnO_x(5)/CeO_2$	$r = kP_{CO}^{0.48}P_{O_2}^{0.016}$	73.8
$CuO(5)$–$MnO_x(5)/CeO_2$	$r = kP_{CO}^{0.69}P_{O_2}^{0.004}$	49.5

dependency of 0.48–0.72 of these catalysts indicates that the reaction probably goes through an intermediate formed by adsorption of CO on the catalyst surface, which is consistent with the FTIR results (Fig. 3), while the O_2 pressure dependency of very close to 0 (0.004–0.043) indicates that gaseous O_2 is not directly involved in the reaction. These power orders of reactants are comparable to the findings of the

$CuO/Ce_{1-x}Cu_xO_{2-\delta}$ catalyst in our previous work [9], except that the CuO(5)/MnO_x(5)/CeO_2 catalyst has a lower CO pressure dependency (0.48) than that of MnO_x(5)/CuO(5)/CeO_2 (0.72) and CuO(5)–MnO_x(5)/CeO_2 catalyst (0.69). In other words, the CuO(5)/MnO_x(5)/CeO_2 possesses stronger CO adsorption ability than that of the MnO_x(5)/CuO(5)/CeO_2 and the CuO(5)–MnO_x(5)/CeO_2 catalysts, which is closely related to its largest amount of Cu^+ as shown in Table 1 derived from XPS result. It should be noted that the kinetic study was carried out at 80 °C, which implies a limited temperature window. The reaction orders (particularly for CO) may change if the kinetic study could be conducted at a wider temperature range (e.g. 50–120 °C), by which more general rate expressions would be obtained.

The Arrhenius plots of CO reaction rates over all the CuO–MnO_x–CeO_2 catalysts are also shown in Fig. 4c, from which their reaction activation energies (E_a) are calculated. The activation energies are 51.8 ($R^2 = 0.998$), 73.8 ($R^2 = 0.980$) and 49.5 kJ mol^{-1} ($R^2 = 0.992$) for the MnO_x(5)/CuO(5)/CeO_2, CuO(5)/MnO_x(5)/CeO_2, and CuO(5)–MnO_x(5)/CeO_2 catalysts, respectively. The highest activation energies on the CuO(5)/MnO_x(5)/CeO_2 suggest that it is less active than the MnO_x(5)/CuO(5)/CeO_2 and CuO(5)–MnO_x(5)/CeO_2 catalysts, which seems to contradict the fact that the CuO(5)/MnO_x(5)/CeO_2 possesses the highest CO adsorption ability. Nevertheless, it reflects the fact that the adsorption bond energy between CO and catalyst surface is very strong in the CuO(5)/MnO_x(5)/CeO_2, which is disadvantageous to CO transfer and surface reaction thus resulting in its highest activation energy [13].

By comparing the rate expressions over these three catalysts, it is believed that the CO oxidation over these three catalysts follows the same pathways. These power rate expressions, particularly the zeroth order dependence on O_2 pressure, suggests that Mars–van Krevelen (M–K) reaction model is more favorable over these catalysts, similar to the findings obtained by our previous study over a CuO/$Ce_{1-x}Cu_xO_{2-\delta}$ catalyst for CO oxidation [9]. However, the classical Langmuir–Hinshelwood (L–H) model was also applied for CO oxidation over Cu-based catalysts [10, 42] with a reaction order of O_2 pressure of near zero (0–0.12). Actually, the rate equation based on the L–H model could also lead to a zeroth reaction order with respect to O_2 pressure if one assumes that the adsorption of O_2 on the catalyst surface is dominant and near-saturated. Therefore, L–H reaction model could not be ruled out at present and the question remains open.

Catalytic performance

A comparison of CO oxidation performance over three types of CuO–MnO_x–CeO_2 catalysts as well as CuO/CeO_2, MnO_x/CeO_2 and CeO_2 support is shown in Fig. 5. The MnO_x/CeO_2 shows relatively higher CO conversion compared to pure CeO_2 in the temperature range investigated, which indicates that the MnO_x species may promote the release of oxygen species from CeO_2. The CuO-containing catalysts exhibit much higher activities for CO oxidation than other CuO-free catalysts, suggesting that CuO species play a much more important role in CO oxidation since CuO can provide the Cu^+ sites for CO adsorption as shown in Fig. 3. In order to obtain more intrinsic reactivity of these catalysts, the catalytic performances of

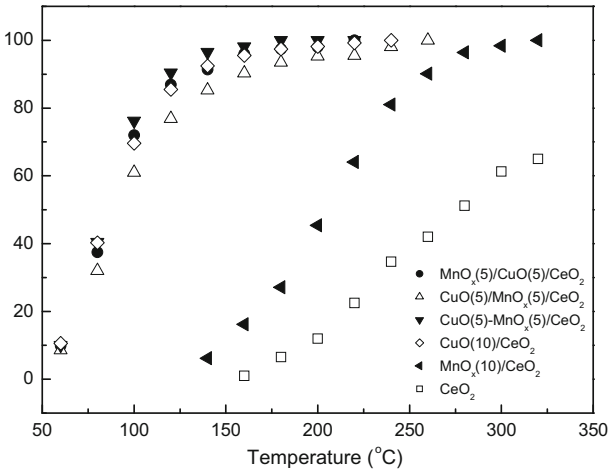

Fig. 5 CO oxidation over various catalysts. CO oxidation experiment conditions: catalyst weight 100 mg (100–120 mesh), feed gas 1 % CO + 1 % O_2 + 98 % N_2, flow rate 80 ml min^{-1}, space velocity 48,000 ml g_{cat}^{-1} h^{-1}

these catalysts are normalized to specific reaction rate in unit of μmol g Cu s^{-1}. As shown in Table 3, the specific reaction rate of CuO-based catalyst decreased following the sequence of CuO(5)–MnO_x(5)/CeO_2 > MnO_x(5)/CuO(5)/CeO_2 ≈ CuO(10)/CeO_2 > CuO(5)/MnO_x(5)/CeO_2. It could be concluded that changing the impregnation sequence of CuO and MnO_x species on CeO_2 support has obvious influence on the catalytic performance. Interestingly, even though CuO(5)/MnO_x(5)/CeO_2 has the highest Cu^+ contents revealed by XPS (Fig. 2b; Table 1), its CO oxidation activity is lowest among three types of CuO–MnO_x–CeO_2 catalyst. This observation indicates that the amount of Cu^+ in CuO–MnO_x–CeO_2 catalysts is not the only factor influencing the catalytic activity of CO oxidation. Based on the results summarized in Table 3, there are probably four main factors that influence the catalytic activity. The first one is the CuO dispersion. As reported by Avgouropoulos et al. [43, 44], the best activity of CuO–CeO_2 catalyst prepared by urea nitrates combustion method compared to those prepared by the co-precipitation and impregnation method is related to the formation of well-dispersed copper oxide species in strong interaction with ceria particles and the absence of bulk CuO in weak interaction with the ceria support. As evidenced by the XRD results (Fig. S1), the aggregation of copper species on the surface of ceria may be disadvantageous to the CO oxidation of the MnO_x(5)/CuO(5)/CeO_2 and CuO(5)/MnO_x(5)/CeO_2 catalyst while the CuO species in CuO(5)–MnO_x(5)/CeO_2 are highly dispersed. The second one is the amount of oxygen vacancies created in these catalysts. Liu et al. [45] investigated the influence of four preparation methods and obtained the best activity from the chelating preparation that favors the formation of defects into the ceria structure and enhances redox cycle between Cu and Ce. As confirmed by Raman spectroscopy (Fig. 1) and the amount of O_{ads} derived from XPS results (Table 1), MnO_x (5)/CuO(5)/CeO_2 has the highest amount of oxygen vacancies, while the

Table 3 Summary of characterization, kinetic and catalytic results over $CuO–MnO_x–CeO_2$ catalysts

Catalyst	CuO dispersion (XRD)	A_{612}/A_{462}	H_2 consumption amount (μmol g^{-1})	The O_{ads} amount (%)	Cu^+ amount (%)	CO reaction order	E_a (kJ mol^{-1})	Specific reaction rate[a] (μmol g_{Cu} s^{-1})
$MnO_x(5)/CuO(5)/CeO_2$	Low	0.74	1300	46.3	58.1	0.72	51.8	55.8
$CuO(5)/MnO_x(5)/CeO_2$	Low	0.51	1370	38.4	76.0	0.48	73.8	47.6
$CuO(5)–MnO_x(5)/CeO_2$	High	0.71	1530	40.1	60.2	0.69	49.5	60.1

[a] Reaction temperature = 80 °C

$CuO(5)/MnO_x(5)/CeO_2$ catalyst has the lowest. It could be deduced that the high amount of oxygen vacancy in $MnO_x(5)/CuO(5)/CeO_2$ could compensate the weakness of its low CuO dispersion and poor reducibility, result in only a little higher apparent activation energy (51.8 kJ mol^{-1}) than that of $CuO(5)–MnO_x(5)/CeO_2$ (49.5 kJ mol^{-1}) catalyst. The third one is the reducibility properties as evidenced by H_2-TPR result (Table 2). The co-impregnation of CuO and MnO_x species in $CuO(5)–MnO_x(5)/CeO_2$ catalyst enhances the reactivity of lattice oxygen which is expected to play an important role in determining the redox behavior and are more facile to extract the oxygen from CeO_2 supported than $MnO_x(5)/CuO(5)/CeO_2$ and $CuO(5)–MnO_x(5)/CeO_2$ as demonstrated by H_2-TPR results. Last but not least, the amount of Cu^+ species, as confirmed by XPS, is also a factor. The $CuO(5)/MnO_x(5)/CeO_2$ has the highest amount of Cu^+ adsorption sites, which is a very important factor contributed to CO oxidation. It was confirmed that Cu^+ species are the main adsorptive and active centers of CO which is very important for CO oxidation, as the activation barrier of CO molecules could be significantly lowered [9]. However, the $CuO(5)/MnO_x(5)/CeO_2$ catalyst has a relatively suppressed activity compared to the other two $CuO–MnO_x–CeO_2$ catalysts, which could be related to the lowest amount of oxygen vacancy, poor reducibility and strongest CO adsorption ability, thus resulting in the lowest reaction order of 0.47. In summary, all these factors such as CuO dispersion, the amount of oxygen vacancy, reducibility and Cu^+ content could be collectively dedicated to the catalytic activity for CO oxidation, which may account for the best catalytic performance of $CuO(5)–MnO_x(5)/CeO_2$ compared to $MnO_x(5)/CuO(5)/CeO_2$ and $CuO(5)/MnO_x(5)/CeO_2$ catalyst. Based on these results, the CuO dispersion and the amount of oxygen vacancy seems to be more important in the catalytic activities for $CuO–MnO_x–CeO_2$ since the highly dispersed CuO species could produce more active sites, accelerating the mobility of lattice oxygen, which was advantageous to enhance its catalytic activity.

Conclusions

This work demonstrates that different impregnation sequences of CuO and MnO_x have a remarkable effect on the CO oxidation activity of $CuO–MnO_x–CeO_2$ catalysts. The different ways of MnO_x doping in the catalysts lead to significant modifications in the CuO dispersion, reducibility properties, the amount of oxygen vacancy and Cu^+ content in the catalysts. Among these catalysts, $CuO–MnO_x/CeO_2$ has the best CO oxidation performance, which could be ascribed to the highest CuO dispersion and the best reducibility or oxygen mobility along with moderate amount of oxygen vacancy and Cu^+ on the catalyst surface. The kinetic study for CO oxidation performed over representative catalysts shows that the partial pressure dependency is 0–1 for CO and 0 for O_2, which could be interpreted by a Mars–van Krevelen type mechanism over these catalysts. This work demonstrates a relationship between the structural property (such as CuO dispersion, the amount of oxygen vacancy, reducibility, the Cu^+ content) and kinetics as well as catalytic behavior for CO oxidation over $CuO–MnO_x–CeO_2$ catalyst.

Acknowledgments This work is financially supported by Public Welfare Project of Zhejiang Province (Grant No. 2013C37086), Open Research Fund of Top Key Discipline of Chemistry in Zhejiang Provincial Colleges and Key Laboratory of the Ministry of Education for Advanced Catalysis Materials (Zhejiang Normal University, Grant No. ZJHX201414) and National Science Foundation of China (Grant No. 21173195).

References

1. Hornés A, Hungría AB, Bera P, López Cámara A, Fernández-García M, Martínez-Arias A, Barrio L, Estrella M, Zhou G, Fonseca JA, Hanson J, Rodriguez JA (2010) J Am Chem Soc 132:34–35
2. Cámara AL, Kubacka A, Schay Z, Koppány Z, Martínez-Arias A (2011) J Power Sources 196:4364–4369
3. Laguna OH, Hernández WY, Arzamendi G, Gandía LM, Centeno MA, Odriozola JA (2014) Fuel 118:176–185
4. Widmann D, Hocking E, Behm RJ (2014) J Catal 317:272–276
5. Liu HH, Wang Y, Jia AP, Wang SY, Luo MF, Lu JQ (2014) Appl Surf Sci 314:725–734
6. Li GN, Li L, Yuan Y, Shi JJ, Yuan YY, Li YS, Zhao WR, Shi JL (2014) Appl Catal B 158–159:341–347
7. Karadeniz H, Karakaya C, Tischer S, Deutschmann O (2013) Chem Eng Sci 104:899–907
8. Avgouropoulos G, Ioannides T (2003) Appl Catal A 244:155–167
9. Jia AP, Hu GS, Meng L, Xie YL, Lu JQ, Luo MF (2012) J Catal 289:199–209
10. Liu W, Flytzani-Stephanopoulos M (1995) J Catal 153:304–316
11. Martínez-Arias A, Fernández-García M, Gálvez O, Coronado JM, Anderson JA, Conesa JC, Soria J, Munuera G (2000) J Catal 195:207–216
12. Luo MF, Ma JM, Lu JQ, Song YP, Wang YJ (2007) J Catal 246:52–59
13. Teng ML, Luo LT, Yang XM (2009) Microporous Mesoporous Mater 119:158–164
14. Chen YZ, Liaw BJ, Huang CW (2006) Int J Hydrog Energy 31:427–435
15. Chen YZ, Liaw BJ, Huang CW (2006) Appl Catal A 302:168–176
16. Sirichaiprasert K, Luengnaruemitchai A, Pongstabodee S (2007) Int J Hydrog Energy 32:915–926
17. Li J, Zhu PF, Zuo SF, Huang QQ, Zhou RX (2010) Appl Catal A 381:261–266
18. Li J, Zhu PF, Zuo SF, Zhou RX (2011) J Power Sources 196:9590–9598
19. Gong L, Luo LT, Wang R, Zhang N (2012) J Chil Chem Soc 57:1048–1053
20. Peng CT, Lia HK, Liaw BJ, Chen YZ (2011) Chem Eng J 172:452–458
21. Gong L, Huang Z, Luo LT, Zhang N (2014) Reac Kinet Mech Cat 111:489–504
22. Tang X, Xu Y, Shen W (2008) Chem Eng J 144:175–180
23. Zhang W, Wang A, Li L, Wang X, Zhang T (2008) Catal Today 131:457–463
24. Polymath (2008) Prentice Hall, Israel. http://www.polymath-software.com/
25. Du X, Yuan Z, Cao L, Zhang C, Wang S (2008) Fuel Process Technol 89:131–138
26. She Y, Zheng Q, Li L, Zhan Y, Chen C, Zheng Y, Lin X (2009) Int J Hydrog Energy 34:8929–8936
27. Li J, Zhu P, Zuo S, Huang Q, Zhou R (2010) Appl Catal A 381:261–266
28. Kim DH, Cha JE (2003) Catal Lett 86:107–112
29. Pu ZY, Lu JQ, Luo MF, Xi YL (2007) J Phys Chem C 111:18695–18702
30. Weber WH, Hass KC, McBride J (1993) Phys Rev B 48:178–185
31. Gamarra D, Munuera G, Hungría AB, Fernández-García M, Conesa JC, Midgley PA, Wang XQ, Hanson JC, Rodriguez JA, Martínez-Arias A (2007) J Phys Chem C 111:11026–11038
32. McBride JR, Hass KC, Poindexter BD, Weber WH (1994) J Appl Phys 76:2435–2441
33. Wang X, Rodriguez JA, Hanson JC, Gamarra D, Martínez-Arias A, Fernández-García M (2005) J Phys Chem B 109:19595–19603
34. Sultana A, Sasaki M, Hamada H (2012) Catal Today 185:284–289
35. Caputo T, Lisi L, Pirone R, Russo G (2008) Appl Catal A Gen 348:42–53
36. Fang J, Bi X, Si D, Jiang Z, Huang W (2007) Appl Surf Sci 253:8952–8961
37. Burroughs P, Hamnett A, Orchard AF, Thornton G (1976) J Chem Soc Dalton Trans 17:1686–1698
38. Tang X, Zhang B, Li Y, Xu Y, Xin Q, Shen W (2005) Appl Catal A Gen 288:116–125
39. Li J, Zhu P, Zuo S, Huang Q, Zhou R (2010) Appl Catal A Gen 381:261–266

40. Liu L, Yu Q, Zhu J, Wan H, Sun K, Liu B, Zhu H, Gao F, Dong L, Chen Y (2010) J Colloid Interface Sci 349:246–255
41. Martínez-Arias A, Hungría AB, Fernández-García M, Conesa JC, Munuera G (2004) J Phys Chem B 108:17983–17991
42. Lee HC, Kim DH (2008) Catal Today 132:109–116
43. Avgouropoulos G, Ioannides T, Matralis H (2005) Appl Catal B 56:87–93
44. Avgouropoulos G, Ioannides T, Matralis H (2006) Appl Catal B 67:1–11
45. Liu ZG, Zhou RX, Zheng XM (2007) J Mol Catal A 267:137–142